Volume 1 | Number 1 | Jan 2013 | Pages 1–100

Nanoscale

www.rsc.org/nanoscale

ROYAL SOCIETY
OF CHEMISTRY

This is an *Accepted Manuscript*, which has been through the Royal Society of Chemistry peer review process and has been accepted for publication.

Accepted Manuscripts are published online shortly after acceptance, before technical editing, formatting and proof reading. Using this free service, authors can make their results available to the community, in citable form, before we publish the edited article. We will replace this *Accepted Manuscript* with the edited and formatted *Advance Article* as soon as it is available.

You can find more information about *Accepted Manuscripts* in the **Information for Authors**.

Please note that technical editing may introduce minor changes to the text and/or graphics, which may alter content. The journal's standard **Terms & Conditions** and the **Ethical guidelines** still apply. In no event shall the Royal Society of Chemistry be held responsible for any errors or omissions in this *Accepted Manuscript* or any consequences arising from the use of any information it contains.

Silica-coated bismuth sulfide nanorods as multimodal contrast agents for

non-invasive visualization of gastrointestinal tract

Xiaopeng Zheng,[1,2,§] Junxin Shi,[1,3,§] Yang Bu,[2] Gan Tian,[1] Xiao Zhang,[1] Wenyan Yin,[1] Bifen Gao,[3] Zhiyong Yang,[2] Zhongbo Hu,[2] Xiangfeng Liu,[2] Liang Yan,[1,] Zhanjun Gu,[1,*] and Yuliang Zhao[1,*]*

[1] CAS Key Laboratory for Biomedical Effects of Nanomaterials and Nanosafety, Institute of High Energy Physics, Chinese Academy of Sciences, Beijing 100049, P. R. China

[2] College of Materials Science and Optoelectronic Technology, University of Chinese Academy of Sciences, Beijing 100049, P. R. China

[3] Department of Applied Chemistry, College of Materials Science & Engineering, Huaqiao University, Xiamen 361021, P. R. China

[§] These authors contributed equally.

Corresponding author: yanliang@ihep.ac.cn, zjgu@ihep.ac.cn, and zhaoyuliang@ihep.ac.cn

ABSTRACT

Non-invasive and real-time imaging of gastrointestinal (GI) tract is particular desirable for research and clinical studies of patients with symptoms arising from the gastrointestinal diseases. Here, we designed and fabricated the silica-coated bismuth sulfide nanorods ($Bi_2S_3@SiO_2$ NRs) for non-invasive spatial-temporally imaging of GI tract. The Bi_2S_3 NRs were synthesized by a facile solvothermal method and then coated with a SiO_2 layer for improving their biocompatibility and stability in the harsh environments of GI tract, such as the stomach and the small intestine. Due to their strong X-ray- and near infrared- absorption abilities, we demonstrate that, following oral administration in mice, the $Bi_2S_3@SiO_2$ NRs can be used as a dual-modal contrast agent for real-time and non-invasive visualization of NRs distribution and GI tract *via* both X-ray computed tomography (CT) and photoacoustic tomography (PAT) techniques. Importantly, integration of PAT with CT provides complementary information on anatomic detail with high spatial resolution. In addition, we use *Caenorhabditis Elegans* (*C. Elegans*) as a simple model organism to investigate the biological response of $Bi_2S_3@SiO_2$ NRs by oral administration. The results indicate that these NRs can pass through the GI tract of *C. Elegans* without inducing notably toxicological effects. The above results suggest that $Bi_2S_3@SiO_2$ NRs pave an alternative way for fabrication of the multi-modal contrast agents which integrate CT and PAT modality for direct and non-invasive visualization of GI tract with low toxicity.

Keywords: X-ray computed tomography, photoacoustic tomography, gastrointestinal tract, Bi_2S_3 nanorods, *Caenorhabditis Elegans*

Introduction

Recently, the diseases of gastrointestinal (GI) tract are very commonly observed in clinical practices [1, 2]. Hence, visual examinations of the anatomy and pathology of the GI tract are often mandatory in the diagnosis of GI diseases to ensure that the patients can receive less invasive treatment and have a good quality of life [3]. For such purposes, non-invasive imaging modalities including ultrasound (US), X-ray computed tomography (CT), positron emission tomography (PET), as well as magnetic resonance imaging (MRI) are the powerful tools because they can provide clinicians with significant insights into the GI disease status, treatment efficacy and patient's prognosis [4-8]. However, in lower GI tract (especially small intestine), thus far, it is still difficult yet imperative to evaluate the symptoms and visualize anatomy and pathology due to the length, complex loops, and peristalsis [3, 9]. Currently, barium sulphate suspension has been routinely used for X-ray contrast enhancement of small investing tract in clinic. Unfortunately, both the intrinsic insolubility and the undesired characters make it not suitable for the patients with GI perforation and intestinal obstruction [10]. Another commonly used contrast agent for GI tract is iodine-based molecules. However, because of the limited X-ray absorption efficiency of iodine, large doses of iodine-based contrast agent is required in daily use, which largely causes serious iodine hypersensitivity reaction in patients [11, 12]. Furthermore, it is rather difficult for the above two kinds of contrast agents to permit the dynamic imaging of small intestine, which is highly desired since it leads to better understanding of real-time biological processes in a variety of physiological or pathological conditions [13, 14]. Therefore, it is necessary to develop new contrast agents which are able to depict the small intestinal lumen, bowel wall, and surrounding structures, and provide reliable extraluminal information.

Along with the development of nanoparticles in the field of diagnostics and therapy, much effort has been devoted to design and fabricate the high-performance orally administered contrast agents for small intestine imaging to achieve the aim of the sensitive and fault-free accurate diagnosis [15-19]. For example, near-infrared (NIR) quantum dots formed by the self-assembly of low molecular weight heparin-deoxycholic acid was used for noninvasive images of the GI tract and evaluation of their absorption after oral administration to the mice [20]. Magnetic nanoparticles and rare-earth doped upconversion nanoparticles have also been applied as the multi-modal contrast agents for direct visualization of GI tract with low systemic toxicity [21]. In recent years, bismuth-based nanomaterials (such as Bi_2S_3 nanoparticles, Bi_2S_3 nanodots, Bi_2S_3 nanorods (NRs), and Bi_2Se_3 nanoplates) which conveniently integrate a broad range of clinically relevant functionalities have stimulated an upsurge

of interest because of their applications as drug delivery platform, biosensor, injectable CT contrast agent, and even as the therapy agents in the biomedical area [22-31]. Bismuth is thought to be the most biocompatible heavy metal and its compounds are the old drugs that have enjoyed great popularity for GI diseases therapy, known as "bismuth therapy", for at least three centuries [1, 32]. More importantly, Bi has the larger atomic number (I, 53; Ta, 73; Pt, 78; Bi, 83) and X-ray attenuation coefficient (I, 1.94; Ta, 4.30; Pt, 4.99; Bi, 5.74 cm^2 g^{-1} at 100 keV), hence implying that bismuth-based nanomaterials can also be used as the contrast agent for CT imaging *in vivo*, which may simultaneously reduce the required dose and allow more flexibility in the clinical setting [33, 34]. In our previous study, we have evaluated the CT performance of Bi_2S_3 NRs and visualized their distribution in mice using the whole-body CT scanning [35]. Our result indicated that Bi_2S_3 NRs showed greatly enhanced CT signal compared to iopromide. As a result, we suppose that Bi_2S_3 NRs also can be used for the study of lower GI tract.

Due to the intrinsic advantages and shortcomings of each medical imaging technique, information achieved from single-modal imaging of GI tract usually cannot satisfy the higher requirement to directly visualize GI tract [21, 36-38]. Therefore, incorporation of multiple imaging approaches into one nanostructure, known as "all-in-one" system, for spatial-temporally diagnostics is highly desirable for the GI tract imaging [39-41]. Photoacoustic tomography (PAT) is a NIR triggered non-invasive and non-ionizing technique which can generate real-time, high resolution scans, and 3D reconstructions. It thus has been widely used for "listening" of blood vessels, tumors, and organs [13, 42-44]. Inspired by the crucial status of fault-free diagnosis of GI diseases, the PAT is greatly welcomed to achieve accurate synergistic imaging outcomes. The PAT/PET bimodality imaging of intestine with frozen nanonaps conjugated with ^{64}Cu was exploited recently by F. Lovell *et al* [37]. Considering these advantages, fusion of PAT with CT by using bismuth-based nanoparticles is highly desirable for direct visualization of GI tract with no depth limitation and remarkable resolution. Here, we designed and prepared silica-coated bismuth sulfide nanorods ($Bi_2S_3@SiO_2$ NRs) as a multi-modal contrast agent for noninvasive and real-time imaging of the GI tract and direct visualization of the NRs passing process in the gastrointestine (Scheme 1). By coating Bi_2S_3 NRs with a thin film of silica, the as-made $Bi_2S_3@SiO_2$ NRs exhibited high aqueous solubility, well biocompatibility and stability in the harsh environments of the stomach and intestinal tract. When exposing *Caenorhabditis Elegans* (*C. Elegans*) to $Bi_2S_3@SiO_2$ NRs, it was found that these NRs could avoid systemic absorption and pass safely through their GI tract. We then performed a series of *in vitro* experiments to quantitate the CT and photoacoustic (PA) signals produced by $Bi_2S_3@SiO_2$ NRs as

well as *in vivo* experiments to understand their utility as a multi-modality contrast agent for the non-invasive and real-time imaging of the lower GI tract and the passing process of NRs in the GI tract.

Experimental section

Materials

All reagents were of analytical grade and used as received without further purification. Bismuth neodecanoate, thioacetamide, and D-α-Tocopherol Polyethylene Glycol 1000 Succinate (TPGS) were purchased from Sigma-Aldrich. Oleic acid (OA) and tetraethylorthosilicate (TEOS) were purchased from Alfa Aesar. Oleic amine was supplied by Aladdin Chemical Co. China. Sodium hydroxide (NaOH), ethanol, and cyclohexane were supplied by Beijing Chemical Reagent Co. China. Deionized water was obtained by a recirculating deionized water system (SHRO-plus DI, 18.2 MΩ·cm at 25 $^{\circ}$C).

Synthesis of Bi_2S_3 NRs

The Bi_2S_3 NRs were prepared by a facile solvothermal method according to our previous report [35]. In detail, bismuth neodecanoate (1.45 g) was added to a mixture of oleic acid (20 mL) and ethanol (10 mL) under thorough stirring. Then, 4 mL of oleylamine containing 0.15 g of thioacetamide was quickly added to the above mixture. After vigorous stirring for 30 min, the obtained solution was transferred into a 45-mL Teflon-lined autoclave, sealed and heated at 150 $^{\circ}$C for 10 h. When cooling to room temperature naturally, the precipitates were collected by centrifugation and washed several times with ethanol to remove any possible remnants.

Preparation of TPGS-functionalized Bi_2S_3 NRs

To transfer the OA-coated Bi_2S_3 NRs from an organic phase to an aqueous phase, TPGS as a biocompatible amphiphilic polymer was used to functionalize the as-prepared NRs *via* hydrophilic interaction [45]. In a typical route, 10 mg of TPGS was added into a 25-mL flask which contained 5 mg of OA-Bi_2S_3 NRs and 10 mL of cyclohexane. After stirring at room temperature for 1 h, 10 mL of deionized water was added into the flask and the dispersion was kept in a water bath at 70 $^{\circ}$C for another 3 h. After the evaporation of cyclohexane, the TPGS-functionalized Bi_2S_3 NRs were obtained by centrifugation and then washed with deionized water and ethanol in sequence.

Preparation of thin silica coated Bi_2S_3 NRs

Typically, the TPGS-modified Bi_2S_3 NRs dispersion (10 mL) was added to a solution containing 20 mL of water, 3 mL of ethanol and 150 μL of 2 M NaOH, and then the resulting mixture was heated up to 70 °C under stirring. Afterwards, 20 μL of tetraethylorthosilicate (TEOS) was added dropwise to the mixture and the reaction was maintained for 10 min. The obtained NRs were centrifuged and washed several times with ethanol.

PAT and CT signals of sample measurement

To test the linearity of the photoacoustic signal as a function of $Bi_2S_3@SiO_2$ NRs concentration, 1 mL of $Bi_2S_3@SiO_2$ NRs aqueous suspensions with various concentrations were added into the agar-phantom container and placed in the MOST in vision 128 (iThera) system for PA signal detection. A complete photoacoustic image of the phantom was collected, and the values of the PA signals were acquired by selecting of the region of interest (ROI). For CT signal detection, $Bi_2S_3@SiO_2$ NRs at different concentrations were dispersed in 0.5% agarose gel and placed into 1.5 mL centrifuge tube for *in vitro* CT imaging. CT phantom images of air, water, and samples were acquired using small mice X-ray CT (Gamma Medica-Ideas). The HU value was calculated using the amira 4.1.2 software according to the CT phantom images of air, water, and sample.

Characterization

The morphology and elements mapping of the as-synthesized NRs were characterized by field emission transmission electron microscopes (TEM, Tecnai G^2 F20 U-TWIN operated at 200 kV) coupled with energy dispersive X-ray spectroscopy (EDS) analysis. Powder X-ray diffraction (XRD) patterns of the dried products were measured using a Japan Rigaku D/max-2500 diffractometer with Cu k_α radiation (λ=1.5418 Å). Fourier Transform infrared (FT-IR) spectra were performed on a Fourier transform Bruker EQUINOX55 spectrometer with the KBr pellet technique. The UV-vis absorption spectra were collected using a Hitachi U-3900 spectrophotometer. All photos were acquired by a Nikon D3100 digital camera.

***In vitro* cytotoxicity study**

16HBE (a human bronchial epithelial cell line) was maintained in RPMI 1640 medium supplemented with 10 % fetal bovine serum (FBS) at 37 °C in a humidified atmosphere of 5 % CO_2. Cell viability was determined using a methyl thiazolyl tetrazolium (MTT) method. For cytotoxicity study, 16HBE cells were firstly seeded into 96-well cell-culture plates at 1×10^4 /well. After incubation for 24 h, 100 μL of $Bi_2S_3@SiO_2$ NRs dispersions in RPMI 1640 with various concentrations (1, 5, 10, 20, 50, and 100 μg mL^{-1}) were added, respectively, and the cells were

incubated for another 24 h. Meanwhile, the wells without treatment with $Bi_2S_3@SiO_2$ NRs were regarded as the control. The MTT assay was performed immediately to test the *in vitro* cytotoxicity of $Bi_2S_3@SiO_2$ NRs.

C. Elegans strains and culture

The wild type N_2 strains and Escherichia coli (E. coli) OP50 were prepared according to the standard procedures [46-48]. The *C. Elegans* were cultured at 20 °C in the nematode growth media (NGM) which was spread with E. coli OP50 suspensions to form bacterial lawn. The *C. Elegans* arrested in the L1 larval stage in the absence of food were then transferred onto the prepared NGM with E. coli lawn and cultured at 20 °C in darkness.

C. Elegans lifespan and growth assays

The NGM/OP50 E. coli plates containing 10 μM 5-fluorodeoxyuracile (FUdR) were prepared to prevent growth of progeny. The *C. Elegans* cultured at 20 °C were transferred to FUdR-containing plates with various $Bi_2S_3@SiO_2$ NRs concentrations (0, 1, 10, 100, and 1000 μg mL^{-1}) until reaching the L4 stage. The day of shift marked as day 0 and counted every second day, worms were scored as dead if they did not respond to mechanical stimulation. 3-day old worms (n = 90-120) on regular plates were imaged after these worms were picked onto an agar pad and immobilized with tetramisole hydrochloride (Sigma, USA), and then body lengths were measured by the Image-Pro® Express software.

C. Elegans oxidative stress resistance and thermotolerance

We chose juglone as an oxidative stressor to study the *C. Elegans* oxidative stress resistance capability. Briefly, 3-day old worms (n = 90-120) were washed with M9 buffer and exposed in NGM plates which contains 600 μM juglone (Sigma, St. Louis, MO) immediately, and incubated at 20 °C. The surviving worms were counted. Thermotolerance assays were performed with 3-day old worms which were transferred into 35 °C. After 10 h, the survival rate was counted subsequently.

C. Elegans fluorescence microscopy

Lipofuscin is an endogenous autofluorescent biomarker of aging which accumulates progressively in *C. Elegans* as a result of aging and oxidative degeneration of cellular components. In order to observe autofluorescence, fluorescence images of worms were collected using an inverted fluorescence microscope (Olympus IX73) equipped with 525 nm band-pass filter. The fluorescence

intensities were measured using Image *J* software (NIH Image, Bethesda, MD, USA) by determining the average pixel intensity in the intestine of each nematode.

Animals

The female BALB/c nude mice were purchased from Beijing Vitalriver Experimental Animal Technology Co. Ltd. with body weights about 20 g and housed in stainless steel cages under the standard conditions with a 12 h light/dark cycle. Distilled water and sterilized food for mice were available and libitum. All procedures used in this experiment were under protocols approved by Key Laboratory for Biomedical Effects of Nanomaterials and Nanosafety (Institute of High Energy Physics, CAS).

CT imaging of GI tract *in vivo*

In vivo CT imaging was performed on small mice X-ray CT (Gamma Medica-Ideas). Imaging parameters: field of view (78.92 mm × 78.92 mm), slice thickness 154 μm, effective pixel size 50 μm, tube current 270 μA, tube voltage 80 KV. The reconstruction is done by Filtered Back Projection (FBP) method. The reconstruction kernel used a Feldkamp cone beam correction and Shepp-Logan filter. The CT images were analyzed using amira 4.1.2. The BALB/c nude mice were received $Bi_2S_3@SiO_2$ NRs solution with a concentration of 10 mg mL^{-1} by oral administration prior to imaging. Thereafter, at different intervals, BALB/c nude mice were imaged by a small animal X-ray CT. The mice whole body 360° scan lasted about 10 min.

PAT imaging of GI tract *in vivo*

The BALB/c nude mice were received 300 μL of $Bi_2S_3@SiO_2$ NRs solution (10 mg mL^{-1}) by oral administration prior to imaging. Thereafter, at different intervals, the mice were narcotized. The photoacoustic signals with the laser light range from 750-850 nm excitation were collected using the multispectral optoacoustic tomography (MSOT) (MSOT inVision 128, iThera medical, Germany). The main experimental parameters were 5 wavelengths for each slice from 750 nm to 850 nm, the region of interest (ROI) is 25 mm. The PAT signals before oral administration were recorded as control.

Results and discussion

The Bi_2S_3 NRs with uniform size have been prepared in a large scale *via* a facile solvothermal method. As shown in Fig. 1A and Fig. S1, the OA-Bi_2S_3 NRs are ~10 nm in diameter and ~50 nm in

length. The high-resolution transmission electron microscopy (HRTEM) images (Fig. 1B) of Bi_2S_3 NRs clearly reveal the lattice fringes with the spacing of 0.810 and 0.406 nm, which is in accord with the lattice spacings of the (110) and (001) planes of Bi_2S_3 NRs, respectively [23, 48-51]. XRD depicted in Fig. S2A revealed that all the peaks could be well indexed to the orthorhombic Bi_2S_3 crystal (JCPDS No. 43-1471), indicating that the as-made Bi_2S_3 NRs showed high quality of crystallization. The energy dispersive X-ray spectroscopy (EDS) analysis demonstrated that characteristic bismuth and sulfur signals were clearly detected in Bi_2S_3 NRs, whereas the oxygen, carbon, and copper peaks largely came from carbon-coated copper grid (Fig. 1D). In addition, TEM elemental mapping illustrates that the bismuth (green color) and sulfur (red color) elements are uniformity covered all the NR areas (Fig. 1C). The XPS was further applied to confirm the NRs composition. Two peaks centered at 159.9 eV and 163.8 eV, as shown in Fig. S2B & C, correspond to the Bi $4f_{7/2}$ and Bi $4f_{5/2}$ peaks of Bi^{3+} ions, respectively. The peak located at 161.2 eV is assigned to S^{2+} 2p [22]. No peaks were detected for metallic Bi and other impurities, indicating the high purity of the as-prepared Bi_2S_3 NRs.

In order to make these NPs withstand the harsh conditions of the gastrointestine, the OA-coated Bi_2S_3 NRs were functionalized with TPGS *via* hydrophobic interactions and then coated with a condense silica layer. The FT-IR spectra as shown in Fig. S2D revealed the presence of TPGS on the surface of Bi_2S_3 NRs which indicates that the OA-coated Bi_2S_3 NRs were successfully functionalized by TPGS. Then, a thin layer of silica was grown onto TPGS-Bi_2S_3 NRs using Stöber synthesis to improve the stability of NRs in the harsh environments and further reduce the concern about the release of Bi ions from NRs (Fig. S3). The TEM images showed that all samples were mono-dispersed NRs and covered by a uniform silica shell with an average thickness of ~6 nm (Fig. 2A & B and Fig. S4). Elemental maps performed by high-angle annular dark-field scanning TEM manifested the actual distribution of Bi, S, and Si elements in the NRs, which was consist with the results of EDS analysis (Fig. 2C & D).

Because being composed with Bi which has a higher photoelectric absorption coefficient than those of I, Ba, and Au, $Bi_2S_3@SiO_2$ NRs exhibit an exciting CT contrast performance [34]. This is notably demonstrated from the determined Hounsfield units (HU) values of $Bi_2S_3@SiO_2$ NRs with various concentrations. As shown in Fig. 3A, the HU values linearly increased with the increase of concentrations of $Bi_2S_3@SiO_2$ NRs, and their slope was about 44.56, which is much higher than that of barium sulfate (18.54). In addition, as shown in Fig. S5, the UV-vis-NIR spectrum of the aqueous

solution of $Bi_2S_3@SiO_2$ NRs exhibited a broad absorption in the NIR region (700-1100 nm) since Bi_2S_3 is a thin band-gap (1.3 eV) semiconductor that expand the light absorption to NIR region [52-55]. Similar to NIR light harvesting materials, such as carbon nanotubes, graphene oxide, gold nanoparticles, copper sulphide, $Bi_2S_3@SiO_2$ NRs have the potential for use as a PAT contrast agent. This performance was evidently certified by the fact that PA signals were recorded with different $Bi_2S_3@SiO_2$ NRs concentrations in experiment, and linear correlations between concentration and PA signals were observed, as shown in Fig. 3B. The above results indicate that $Bi_2S_3@SiO_2$ NRs can be employed to design an potential multi-modal contrast agent that integrates CT imaging and PA modality for direct visualization of GI tract, which may obtain more complementary, effective, and accurate information of GI diseases for diagnosis and prognosis.

To assess the suitability of $Bi_2S_3@SiO_2$ NRs for use as an orally administered contrast agent for imaging of the GI tract, we first study the toxicity response of the NRs in biological system, which lays a foundation for designing an oral GI contrast agent. The cellular toxicity of $Bi_2S_3@SiO_2$ NRs was evaluated using 16HBE cell line. After incubation with $Bi_2S_3@SiO_2$ NRs for 24 h, the result of the standard MTT assay exhibited that the cell viability was not influenced by the $Bi_2S_3@SiO_2$ NRs even when concentrations reached up to 100 μg mL^{-1} (Fig. S6). Furthermore, because of the features of the short generation time, the ability to be easily cultured in the laboratory, and the simple digestive tract, *C. Elegans* were used as an animal model to further assess the toxicity of $Bi_2S_3@SiO_2$ NRs and investigate the absorption of NRs from the GI tract (Fig. 4 & Fig. S7-S10). From the bright field images of the *C. Elegans* co-cultivated with $Bi_2S_3@SiO_2$ NRs in Fig. 4A & B, we could observe the uptake of NPs into the gut of *C. Elegans*. As shown in Fig. S7, after exposure to $Bi_2S_3@SiO_2$ NRs at concentrations from 10 to 1000 μg mL^{-1}, no significant lifespan extension or reduced the percentage of survival *C. Elegans* were observed, and this treatment did not noticeably influence the body length of worms compared to the control group (Fig. 4C). As shown in Fig. 4D-H, after 3 days of exposure to $Bi_2S_3@SiO_2$ NRs with different concentrations, the intensities of intestinal autofluorescence were similar with that of the control group, indicating that NRs hardly induce notably effect on the lipofusion level at given concentration. These NRs persisted in the alimentary canal and pass through the intestinal without triggering the toxicity effect to the *C. Elegans*. Moreover, there were no adverse behavioral or weight changes in BALB/c mice over ~ 3 weeks study after oral administration of NRs (Fig. S11). Encouraging by the above results, we further administered $Bi_2S_3@SiO_2$ NRs *via* gavage to mice to investigate the GI imaging performance.

We next examined the utility of $Bi_2S_3@SiO_2$ NRs as a multi-modal contrast agent for non-invasive and real time imaging of the lower GI tract *in vivo* by oral administration of NRs to BALB/c nude mice. We first examined the *in vivo* X-ray CT contrast efficacy of $Bi_2S_3@SiO_2$ NRs, as shown in Fig. 5, 6, & Fig. S12. The 3D-renderings CT images of GI tract were illustrated in Fig. 5 and revealed the process of $Bi_2S_3@SiO_2$ NRs through the GI tract. At 10 min after oral administration, organs including stomach, duodenum, and the first few loops of the small intestine began to be brightened, suggesting the presence of $Bi_2S_3@SiO_2$ NRs in GI tract. After another 20 min, the small intestine was filled with $Bi_2S_3@SiO_2$ NRs and thus was clearly observed. This result was much better than the group treated with $BaSO_4$ (Fig. S13). The sequence and arrangement of the intestinal loops were directly visualized, as shown in Fig. 6 & Movie S1. Besides, the intestinal motility could be captured from CT imaging, as seen in Movie S2. After 60 min, $Bi_2S_3@SiO_2$ NRs had advanced to the end of the small intestine and began to fill the large intestine. Until 100 min after administration, the gastric emptying notably advanced and the small intestine was nearly empty, whereas the large intestine was filled to a large extent. Importantly, 220 min later, $Bi_2S_3@SiO_2$ NRs were found to be excreted in the faeces, which indicated their stability in the GI tract and being directly drained to external *via* defecation. Moreover, the faeces possessed normal morphology and strong CT contrast, confirming that the $Bi_2S_3@SiO_2$ NRs could not lead to the GI dysfunction. In addition, the 3D reconstruction method provided detailed 3D views of the GI anatomy. As expected, the intestine is folded many times, forming several layers that filled the entire abdominal region (Movie S1).

Apart from their application for CT imaging, due to the strong NIR absorption property, $Bi_2S_3@SiO_2$ NRs can also be employed as a contrast agent for non-invasive and real-time PAT imaging of GI tract *in vivo*. As shown in Fig. 7, the cross-sectional PA signals of stomach, small intestine, and large intestine were recorded at different time interval. After oral administration to BALB/c nude mice, $Bi_2S_3@SiO_2$ NRs began to gradually fill the stomach and small intestine in 10 min. It was note that negligible background was detected, which enabled the clear resolution of intestinal structure. After 60 min, $Bi_2S_3@SiO_2$ NRs fully filled the small intestine, making it become much brighter. Accompany with the progression of NRs in GI tract, $Bi_2S_3@SiO_2$ was gradually propagated from the stomach, small intestine through large intestine and, finally, were expelled to external by defecation. Therefore, the as-prepared $Bi_2S_3@SiO_2$ could be potentially served as a dual-modal CT/PAT probe for functional GI tract imaging.

Conclusion

In summary, we have developed a multi-modal contract agent based on $Bi_2S_3@SiO_2$ NRs for non-invasive and real time visualization of GI tract. The Bi_2S_3 NRs with uniform morphology were prepared by a facile solvothermal method, and then coated with a thin SiO_2 layer to improve their dispersion and reduce the concern about the release of Bi ions. Both *in vitro* and *in vivo* studies demonstrated that the as-made $Bi_2S_3@SiO_2$ NRs showed low toxicity, good biocompatibility, and had the ability of withstanding the harsh environments in GI tract. Owing to its high X-ray attenuation and strong optical absorption in the NIR, the $Bi_2S_3@SiO_2$ NRs were applied for CT imaging and PAT imaging of GI tract, realizing the incorporation of the CT with PAT techniques using a single agent. In addition, the sequence and arrangement of the intestinal loops were clearly visualized. The $Bi_2S_3@SiO_2$ NRs as multi-modal contrast agents provide a new avenue to precise imaging of GI tract and improvement of the diagnostic quality of GI examinations in clinical practice.

Acknowledgments

Author contributions

Xiaopeng Zheng and Junxin Shi contributed equally to the work in writing the main manuscript text, performing experiments and preparing figures. Yang Bu, Gan Tian, Xiao Zhang, Wenyan Yin, Bifen Gao, Zhiyong Yang, Zhongbo Hu and Xiangfeng Liu helped to analyze the data and give the constructive discussions. Liang Yan, Zhanjun Gu and Yuliang Zhao designed and supervised the research project and revised this paper. All authors reviewed the manuscript.

References

1.   S. L. Gorbach, *Gastroenterology*, 1990, **99**, 863-875.

2.   X. Yan, R. Wang, Y. Zhao, X. Ma, J. Fang, H. Yan, X. Kang, P. Yin, Y. Hao, Q. Li, J. Dent, J. Sung, D. Zou, S. Johansson, K. Halling, W. Liu and J. He, *BMC Gastroenterol.*, 2009, **9**, 86.

3. P. F. Hahn, D. D. Stark, J. M. Lewis, S. Saini, G. Elizondo, R. Weissleder, C. Fretz and J. Ferrucci, *Radiology*, 1990, **175**, 695-700.

4. L. A. Jelicks, *J. Neuroparasitol.*, 2010, **1**.

5. J. V. Jokerst, *Nat. Nanotechnol.*, 2014, **9**, 569-570.

6. S.-G. Kim, J. Ashe, K. Hendrich, J. M. Ellermann, H. Merkle, K. Ugurbil and A. P. Georgopoulos, *Science*, 1993, **261**, 615-617.

7. R. N. Low and I. R. Francis, *Am. J. Roentgenol.*, 1997, **169**, 1051-1059.

8. C. L. Morgan, W. S. Trought, T. A. Oddson, W. Clark and R. Rice, *Radiology*, 1980, **135**, 129-135.

9. J.-B. Frøkjær, *World J. Gastroenterol.*, 2009, **15**, 160.

10. A. Megibow and M. Bosniak, *Am. J. Roentgenol.*, 1980, **134**, 1273-1274.

11. F. Hallouard, N. Anton, P. Choquet, A. Constantinesco and T. Vandamme, *Biomaterials*, 2010, **31**, 6249-6268.

12. B. Todd, *Geriatr. Nurs.*, 1987, **8**, 341-348.

13. K. Pu, A. J. Shuhendler, J. V. Jokerst, J. Mei, S. S. Gambhir, Z. Bao and J. Rao, *Nat. Nanotechnol.*, 2014, **9**, 233-239.

14. V. Ntziachristos and D. Razansky, *Chem. Rev.*, 2010, **110**, 2783-2794.

15. M. Nakamura, A. Awaad, K. Hayashi, K. Ochiai and K. Ishimura, *Chem. Mater.*, 2012, **24**, 3772-3779.

16. G. Yang, H. Gong, T. Liu, X. Sun, L. Cheng and Z. Liu, *Biomaterials*, 2015, **60**, 62-71.

17. D. Ni, W. Bu, S. Zhang, X. Zheng, M. Li, H. Xing, Q. Xiao, Y. Liu, Y. Hua, L. Zhou, W. Peng, K. Zhao and J. Shi, *Adv. Funct. Mater.*, 2014, **24**, 6613-6620.

18. H. Xing, W. Bu, Q. Ren, X. Zheng, M. Li, S. Zhang, H. Qu, Z. Wang, Y. Hua, K. Zhao, L. Zhou, W. Peng and J. Shi, *Biomaterials*, 2012, **33**, 5384-5393.

19. H. Xing, W. Bu, S. Zhang, X. Zheng, M. Li, F. Chen, Q. He, L. Zhou, W. Peng, Y. Hua and J. Shi, *Biomaterials*, 2012, **33**, 1079-1089.

20. Z. Khatun, M. Nurunnabi, K. J. Cho and Y.-k. Lee, *Carbohydr. Polym.*, 2012, **90**, 1461-1468.

21. Z. Liu, E. Ju, J. Liu, Y. Du, Z. Li, Q. Yuan, J. Ren and X. Qu, *Biomaterials*, 2013, **34**, 7444-7452.

22. K. Ai, Y. Liu, J. Liu, Q. Yuan, Y. He and L. Lu, *Adv. Mater.*, 2011, **23**, 4886-4891.

23.   A. K. Dutta, S. K. Maji, K. Mitra, A. Sarkar, N. Saha, A. B. Ghosh and B. Adhikary, *Sens. Actuators B*, 2014, **192**, 578-585.

24.   J. M. Kinsella, R. E. Jimenez, P. P. Karmali, A. M. Rush, V. R. Kotamraju, N. C. Gianneschi, E. Ruoslahti, D. Stupack and M. J. Sailor, *Angew. Chem. Int. Ed. Engl.*, 2011, **50**, 12308-12311.

25.   J. Li, F. Jiang, B. Yang, X. R. Song, Y. Liu, H. H. Yang, D. R. Cao, W. R. Shi and G. N. Chen, *Sci. Rep.*, 2013, **3**, 1998.

26.   M. Ma, Y. Huang, H. Chen, X. Jia, S. Wang, Z. Wang and J. Shi, *Biomaterials*, 2015, **37**, 447-455.

27.   O. Rabin, J. Manuel Perez, J. Grimm, G. Wojtkiewicz and R. Weissleder, *Nat. Mater.*, 2006, **5**, 118-122.

28.   M. Wang, H. Yin, N. Shen, Z. Xu, B. Sun and S. Ai, *Biosens. Bioelectron.*, 2014, **53** 232-237.

29.   M. H. Yao, M. Ma, Y. Chen, X. Q. Jia, G. Xu, H. X. Xu, H. R. Chen and R. Wu, *Biomaterials*, 2014, **35**, 8197-8205.

30.   H. Yin, B. Sun, Y. Zhou, M. Wang, Z. Xu, Z. Fu and S. Ai, *Biosens. Bioelectron.*, 2014, **51**, 103-108.

31.   X.-D. Zhang, J. Chen, Y. Min, G. B. Park, X. Shen, S.-S. Song, Y.-M. Sun, H. Wang, W. Long, J. Xie, K. Gao, L. Zhang, S. Fan, F. Fan and U. Jeong, *Adv. Funct. Mater.*, 2014, **24**, 1718-1729.

32.   K. D. Mjos and C. Orvig, *Chem. Rev.*, 2014, **114**, 4540-4563.

33.   H. Lusic and M. W. Grinstaff, *Chem. Rev.*, 2013, **113**, 1641-1666.

34.   N. Lee, S. H. Choi and T. Hyeon, *Adv. Mater.*, 2013, **25**, 2641-2660.

35.   J. Liu, X. Zheng, L. Yan, L. Zhou, G. Tian, W. Yin, L. Wang, Y. Liu, Z. Hu and Z. Gu, *ACS Nano*, 2015, **9**, 696-707.

36.   N. Lee, H. R. Cho, M. H. Oh, S. H. Lee, K. Kim, B. H. Kim, K. Shin, T. Y. Ahn, J. W. Choi, Y. W. Kim, S. H. Choi and T. Hyeon, *J. Am. Chem. Soc.*, 2012, **134**, 10309-10312.

37.   Y. Zhang, M. Jeon, L. J. Rich, H. Hong, J. Geng, Y. Zhang, S. Shi, T. E. Barnhart, P. Alexandridis and J. D. Huizinga, *Nat. Nanotechnol.*, 2014, **9**, 631-638.

38.   Z. Liu, J. Liu, R. Wang, Y. Du, J. Ren and X. Qu, *Biomaterials*, 2015, **56**, 206-218.

39.   T. Liu, S. Shi, C. Liang, S. Shen, L. Cheng, C. Wang, X. Song, S. Goel, T. E. Barnhart and W. Cai, *ACS Nano*, 2015, **9**, 950-960.

40.   L. Cheng, J. Liu, X. Gu, H. Gong, X. Shi, T. Liu, C. Wang, X. Wang, G. Liu and H. Xing, *Adv. Mater.*, 2014, **26**, 1886-1893.

41.   R. Lv, C. Zhong, R. Li, P. Yang, F. He, S. Gai, Z. Hou, G. Yang and J. Lin, *Chem. Mater.*, 2015, **27**, 1751-1763.

42.   Z. Zhang, L. Wang, J. Wang, X. Jiang, X. Li, Z. Hu, Y. Ji, X. Wu and C. Chen, *Adv. Mater.*, 2012, **24**, 1418-1423.

43.   Z. Sheng, L. Song, J. Zheng, D. Hu, M. He, M. Zheng, G. Gao, P. Gong, P. Zhang, Y. Ma and L. Cai, *Biomaterials*, 2013, **34**, 5236-5243.

44.   D. Razansky, M. Distel, C. Vinegoni, R. Ma, N. Perrimon, R. W. Köster and V. Ntziachristos, *Nat. Photonics*, 2009, **3**, 412-417.

45.   G. Tian, X. Zheng, X. Zhang, W. Yin, J. Yu, D. Wang, Z. Zhang, X. Yang, Z. Gu and Y. Zhao, *Biomaterials*, 2015, **40**, 107-116.

46.   H. Zhang, X. He, Z. Zhang, P. Zhang, Y. Li, Y. Ma, Y. Kuang, Y. Zhao and Z. Chai, *Environ. Sci. Technol.*, 2011, **45**, 3725-3730.

47.   E. Q. Contreras, M. Cho, H. Zhu, H. L. Puppala, G. Escalera, W. Zhong and V. L. Colvin, *Environ. Sci. Technol.*, 2013, **47**, 1148-1154.

48.   Y. Qu, W. Li, Y. Zhou, X. Liu, L. Zhang, L. Wang, Y. F. Li, A. Iida, Z. Tang, Y. Zhao, Z. Chai and C. Chen, *Nano Lett.*, 2011, **11**, 3174-3183.

49.   R. Chen, M. H. So, C.-M. Che and H. Sun, *J. Mater. Chem.*, 2005, **15**, 4540.

50.   Q. Han, J. Chen, X. Yang, L. Lu and X. Wang, *J. Phys. Chem. C*, 2007, **111**, 14072-14077.

51.   B. Zhang, X. Ye, W. Hou, Y. Zhao and Y. Xie, *J. Phys. Chem. B*, 2006, **110**, 8978-8985.

52.   N. Liang, J. Zai, M. Xu, Q. Zhu, X. Wei and X. Qian, *J. Phys. Chem. A*, 2014, **2**, 4208.

53.   S.-C. Liufu, L.-D. Chen, Q. Yao and C.-F. Wang, *Appl. Phys. Lett.*, 2007, **90**, 112106.

54.   P. K. Panigrahi and A. Pathak, *J. Nanopart.*, 2013, **2013**, 1-11.

55.   Y. Xi, C. Hu, X. Zhang, Y. Zhang and Z. L. Wang, *Solid State Commun.*, 2009, **149**, 1894-1896.

Figure Captions
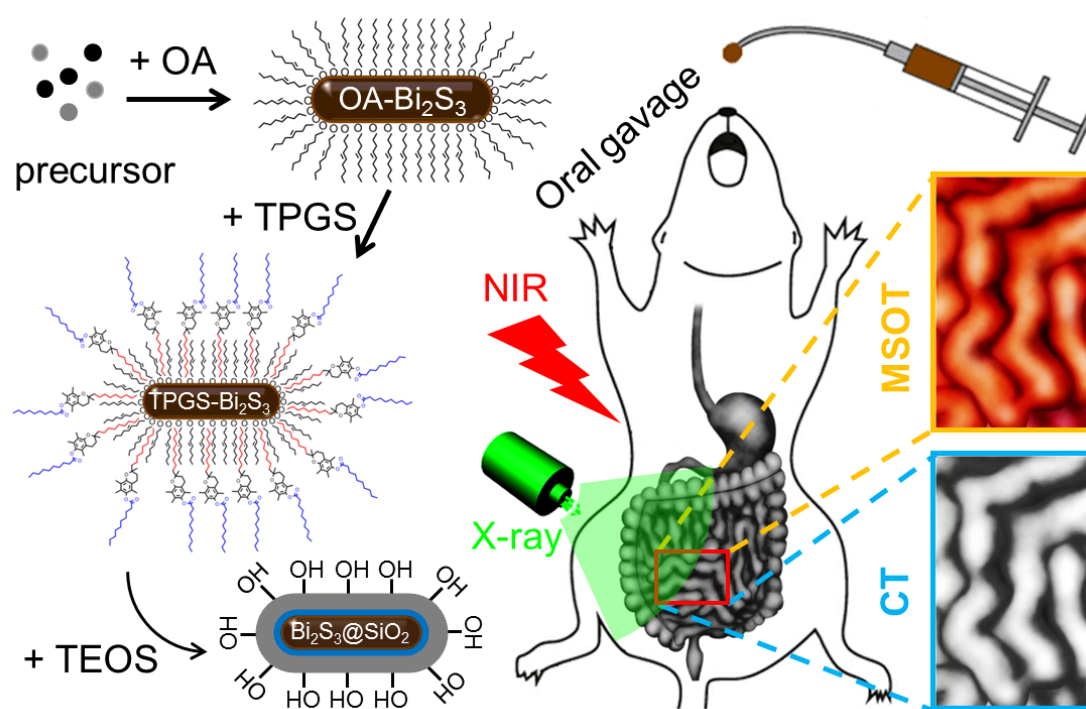
Scheme 1 Schematic illustration of the preparation of $Bi_2S_3@SiO_2$ NRs for bimodal CT/PAT imaging of GI tract principle based on the unique properties of the $Bi_2S_3@SiO_2$ NRs.
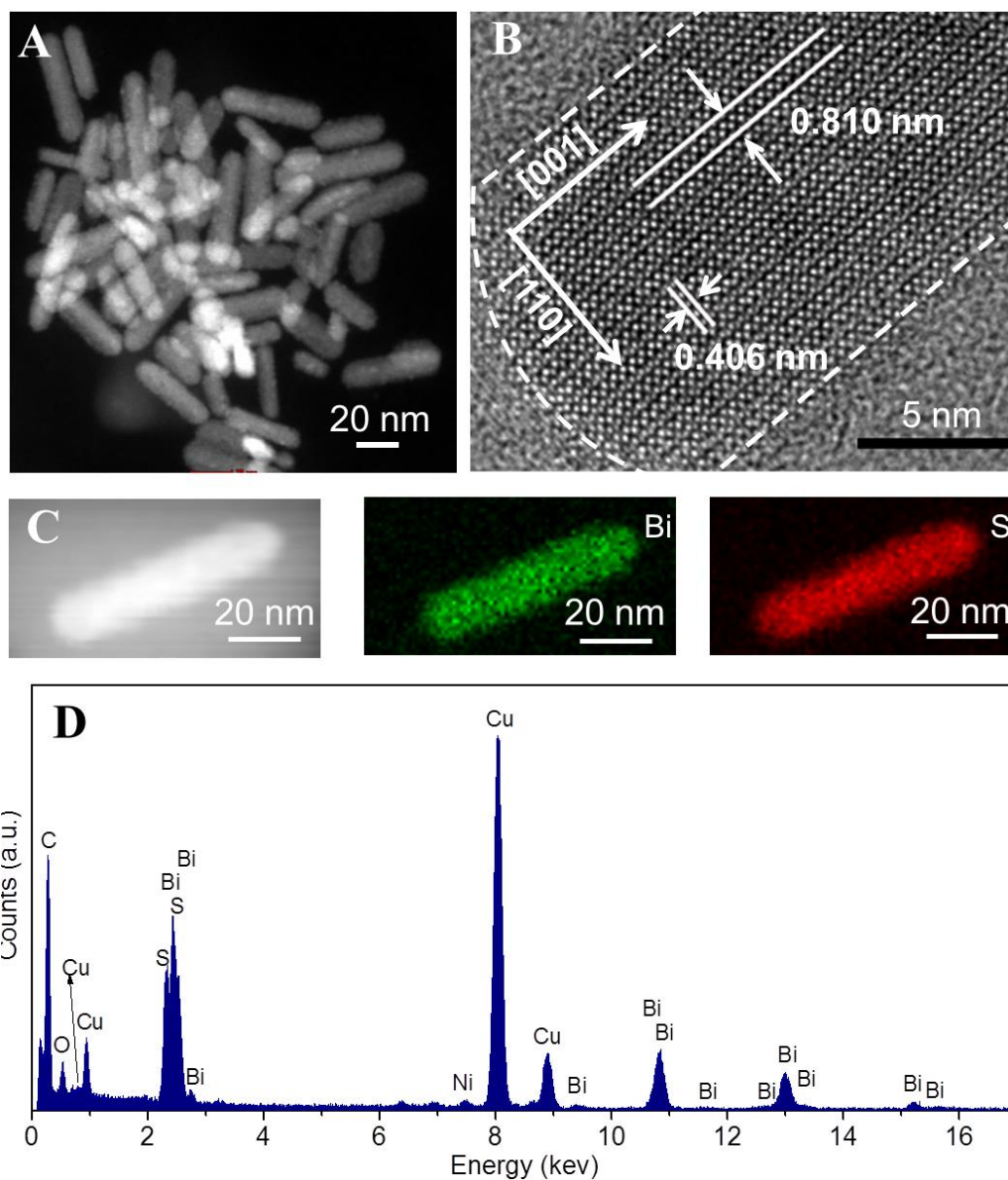
Fig. 1 Characterization of Bi$_2$S$_3$ NRs. (A) HAADF-STEM image and (B) HRTEM image of Bi$_2$S$_3$ NRs prepared by solvothermal method. (C) Corresponding element mapping for Bi and S of as-prepared Bi$_2$S$_3$ NRs. (D) EDS of as-prepared Bi$_2$S$_3$ NRs.

Nanoscale Accepted Manuscript
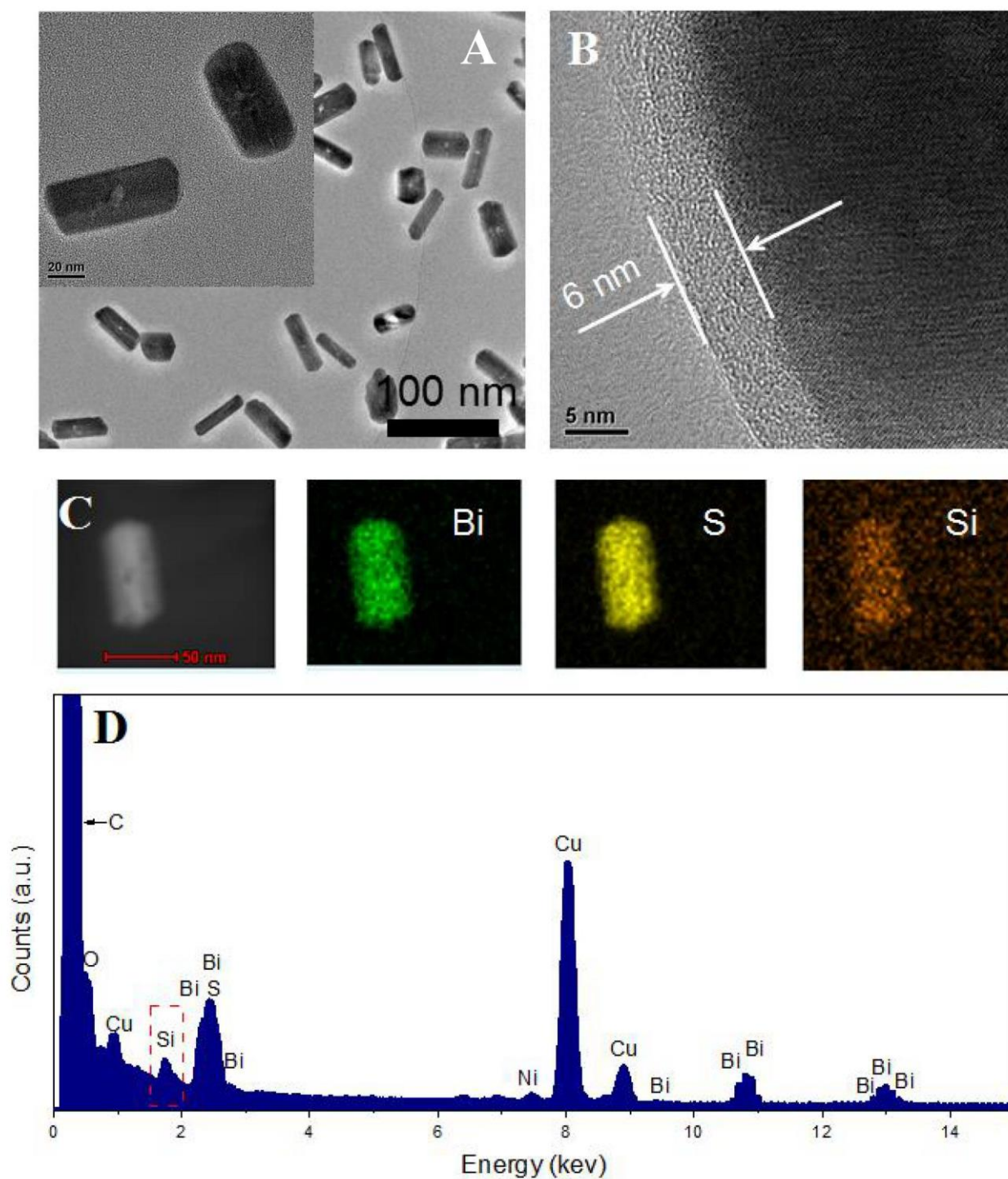
Fig. 2 Characterization of Bi$_2$S$_3$@SiO$_2$ NRs. (A) TEM image and (B) HRTEM image of as-prepared Bi$_2$S$_3$@SiO$_2$ NRs. Inset: HAADF-STEM image of Bi$_2$S$_3$@SiO$_2$ NRs. (C) Corresponding element mapping for Bi, S, and Si of Bi$_2$S$_3$@SiO$_2$ NRs. (D) EDS of Bi$_2$S$_3$@SiO$_2$ NRs.
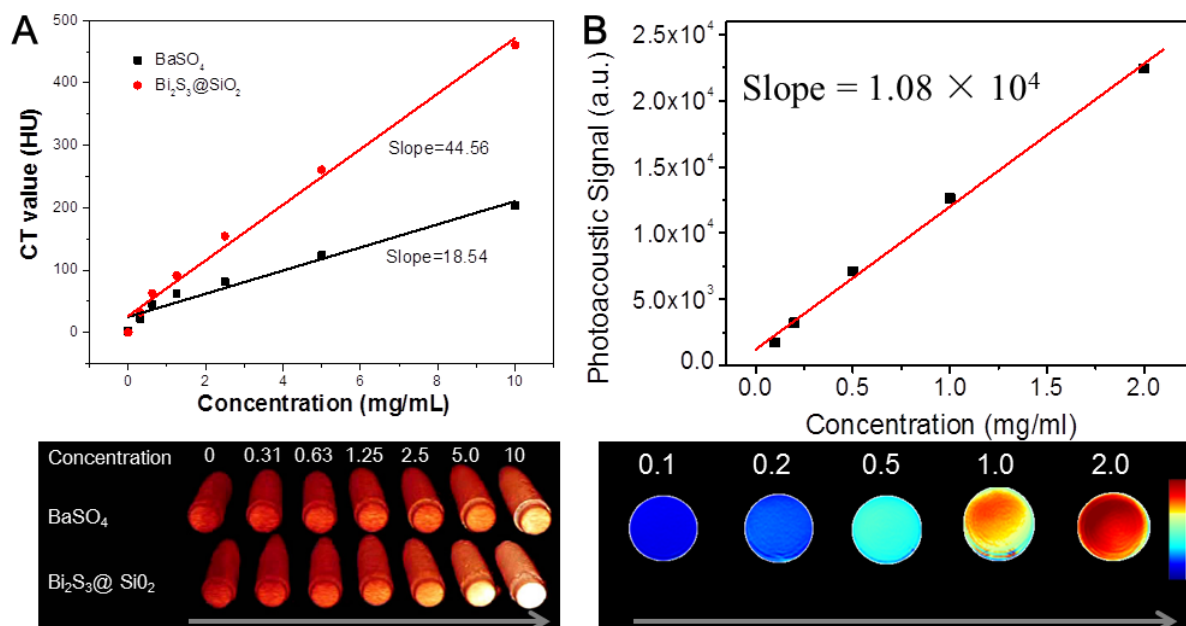
Fig. 3 CT and PAT phantom images of Bi$_2$S$_3$@SiO$_2$ NRs with different concentrations *in vitro*. (A) Plot of Hounsfield units (HU) values and of Bi$_2$S$_3$@SiO$_2$ NRs and BaSO$_4$ suspension versus the samples concentrations and CT phantom images of Bi$_2$S$_3$@SiO$_2$ NRs and BaSO$_4$ suspension samples with different concentrations. (B) Plot of photoacoustic signal versus Bi$_2$S$_3$@SiO$_2$ NRs concentrations and PAT phantom images of Bi$_2$S$_3$@SiO$_2$ NRs aqueous solutions with different concentrations.
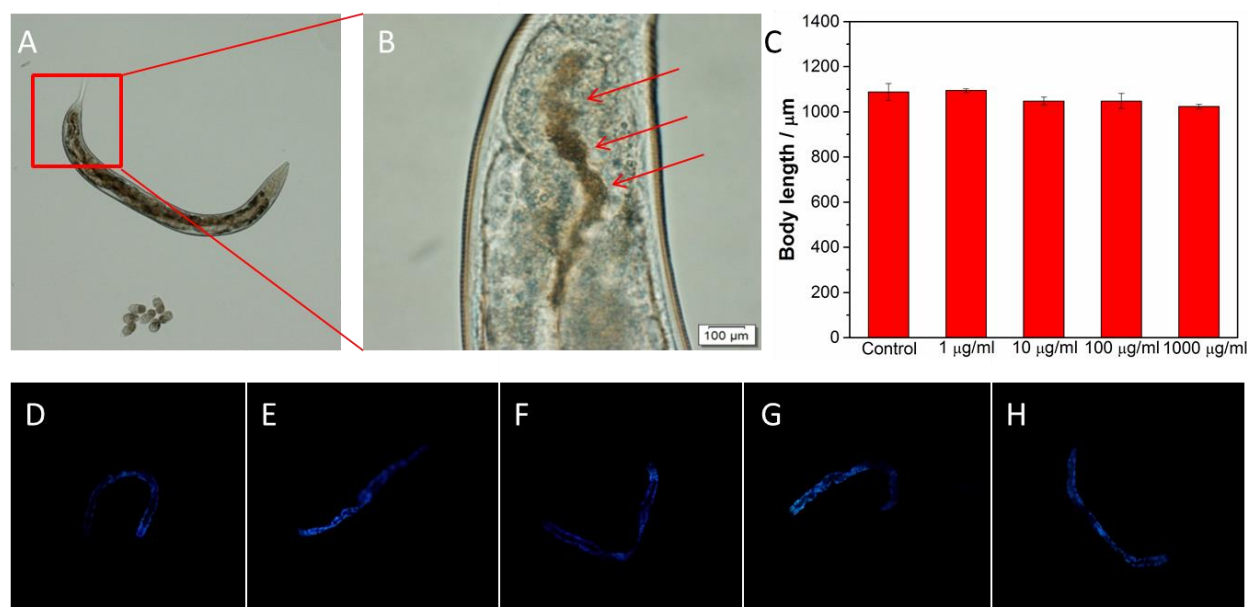
Fig. 4 Biosafety assessment of Bi$_2$S$_3$@SiO$_2$ NRs by *C. Elegans* model. (A) Bright field imaging of NRs distribution in GI tract of *C. Elegans*. Worms feed on NGM plates with Bi$_2$S$_3$@SiO$_2$ NRs (1000 μg mL^{-1}) transferred onto an agar pad after 1 h. (B) The distribution of food contained Bi$_2$S$_3$@SiO$_2$ NRs (red arrows) in the intestines of the worm's tail. (C) Effects of Bi$_2$S$_3$@SiO$_2$ NRs with different concentrations on body length of *C. Elegans*. (D-H) Effects of Bi$_2$S$_3$@SiO$_2$ NRs treatments on the accumulation of lipofuscin in age-synchronized worms. Representative fluorescent images of worms fed with 0, 1, 10, 100, and 1000 μg mL^{-1} Bi$_2$S$_3$@SiO$_2$ NRs, respectively.
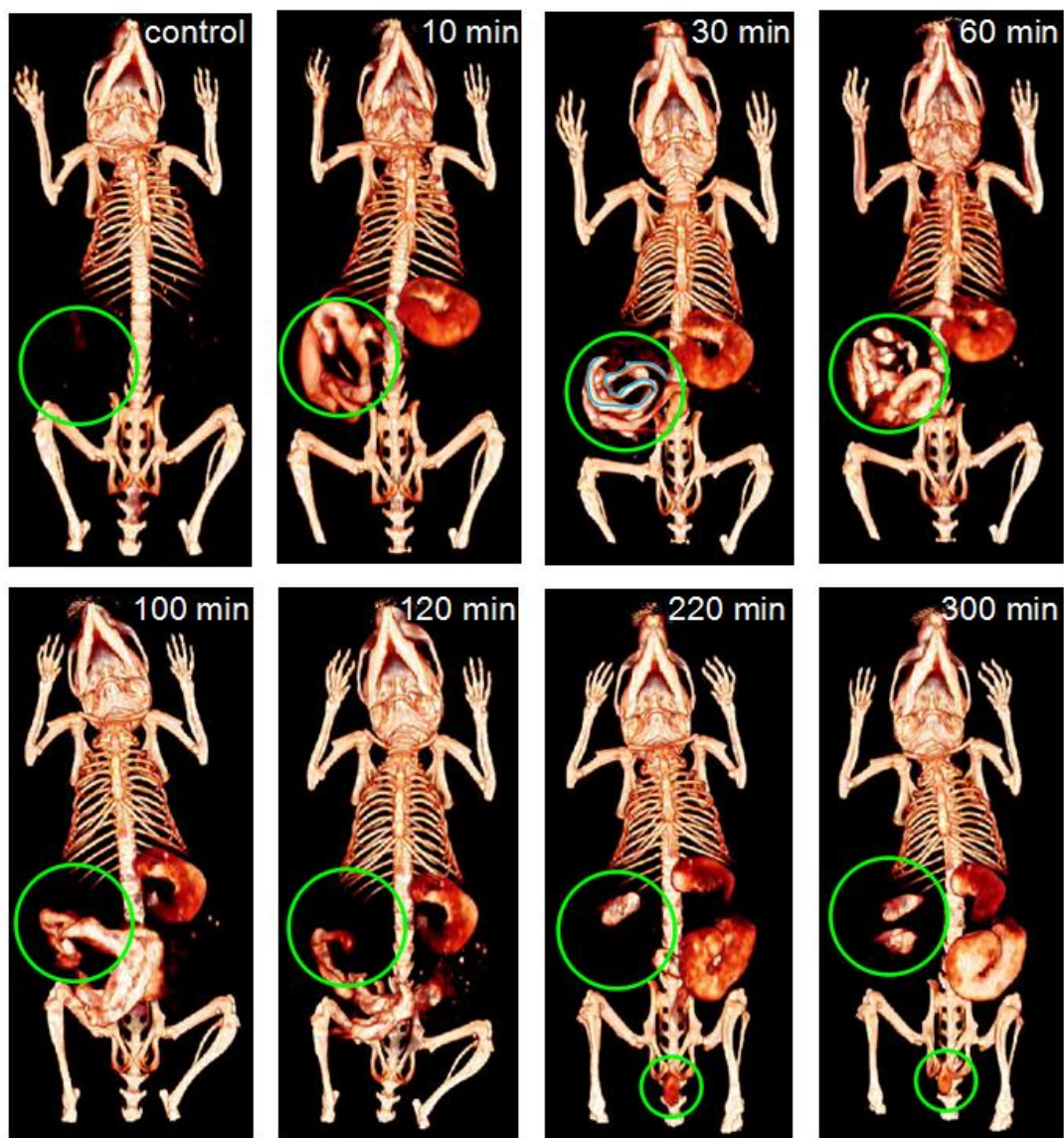
Fig. 5 CT imaging of GI tract *in vivo*. *In vivo* X-ray CT imaging of GI tract in BALB/c nude mice at different intervals after oral administration of $Bi_2S_3@SiO_2$ NRs.
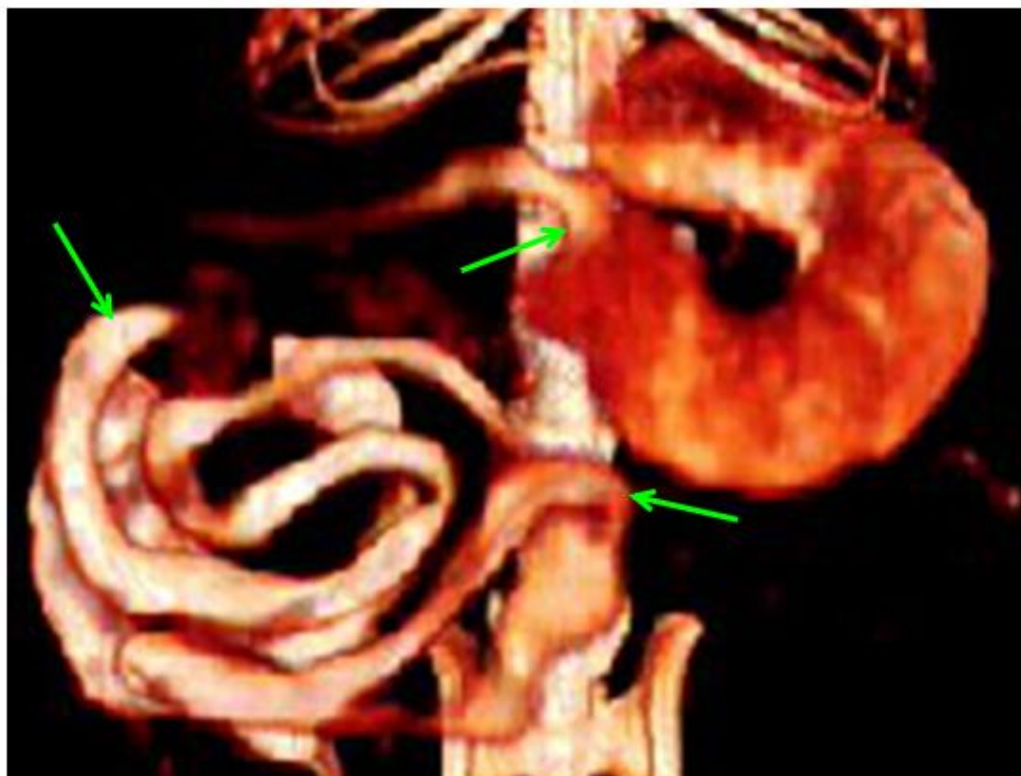
Fig. 6 Enlarged images of CT images of GI tract of mice 30 min post oral administration of Bi$_2$S$_3$@SiO$_2$ NRs.
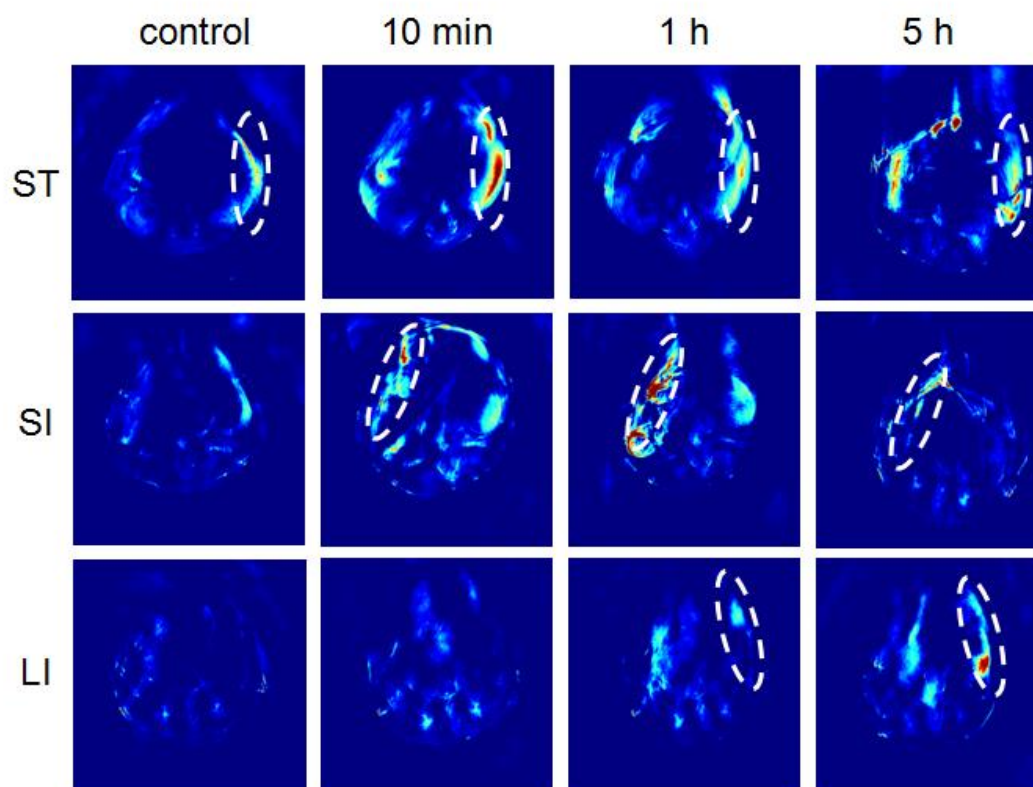
Fig. 7 PAT imaging of GI tract *in vivo*. PAT cross-sectional image of GI tract of BALB/c nude mice at different intervals after oral administration of $Bi_2S_3@SiO_2$ NRs: stomach (ST), small intestine (SI), large intestine (LI).

Table of Contents
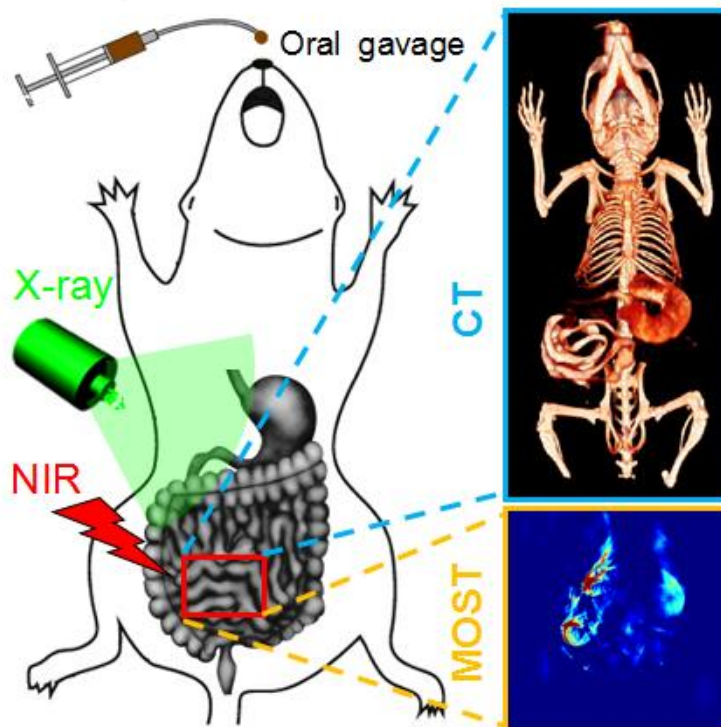
In this paper, we have prepared the $Bi_2S_3@SiO_2$ nanorods designed specifically as binary contrast agents for non-invasive and real-time visualization of gastrointestinal tract *via* achieving X-ray computed tomography and photoacoustic tomography.